DINAME 2017 - Proceedings of the XVII International Symposium on Dynamic Problems of Mechanics
A. T. Fleury, D. A. Rade, P. R. G. Kurka (Editors), ABCM, São Sebastião, SP, Brazil, March 5-10, 2017

Dynamic Modelling and Identification of a Planar PKM with Several Levels of Kinematic Redundancies

João V. C. Fontes, João C. Santos, Hiparco L. Vieira, Maíra M. da Silva

São Carlos School of Engineering (EESC), University of São Paulo (USP)
Av. Trab. Sancarlense, 400, São Carlos-SP, Brazil

joao.fontes@usp.br, joao.cavalcanti.santos@usp.br, hiparcolins@usp.br, maira@sc.usp.br

Abstract: The estimation of parameters used in dynamic models is mandatory for deriving validated models that can be used for motion planning and model-based control strategies. Therefore, a parameter identification procedure based on an optimization problem is proposed to estimate the masses of the components of a 3PRRR manipulator. In this problem, the selection of the excitation trajectories plays an important role in the estimation procedure, once this selection interferes on the amount and quality of data obtained from the manipulator. In order to fulfill these requirements, six different trajectories with different poses are chosen as excitation trajectories. The optimization procedure aims to minimize the difference between the experimental and numerical data. Moreover, detailed kinematic and dynamic models are described. Based on the geometric description of the prototype and its constraints, the inverse kinematic model has been derived. Euler-Lagrange formalism and Lagrange multiplier technique have been used to the dynamic model's derivation. Finally, the comparison between the experimental and numerical data of a triangular trajectory demonstrates the effectiveness of the employed methodology.

Keywords: PKM, dynamic modelling, parameter estimation, optimization, excitation trajectories

INTRODUCTION

Recently, parallel kinematic manipulators have received considerable attention from the scientific community. The main reasons arise from the comparison performed between parallel and serial manipulators. Firstly, on the one hand, serial robots have a payload issue, since each joint needs to deal with all loadings of the subsequent joints, e.g., moving actuators, structural or external forces (Santos et al., 2015). On the other hand, parallel manipulators share the load between all the actuators, which are generally fixed in the base Gosselin and Angeles (1990); Bonev et al. (2003). Secondly, due to the fact that the loads are distributed, parallel manipulators can achieve higher speeds and accelerations, as well as better accuracy (Merlet, 1996). Also, energy consumption ends up being reduced, due to the decrease of required torque to accomplish their objectives (Ruiz et al., 2015). However, parallel manipulators have disadvantages, e.g., presence of singularities and the fact that their models are generally more complex than serial manipulators. These facts may demand rather complex control design strategies (Gosselin and Angeles, 1990; Paccot et al., 2009; Bourbonnais et al., 2015; Lakhal et al., 2016).

Some authors, among them Kotlarski et al. (2009); Mohamed and Gosselin (2005); Cha et al. (2007); Fontes and da Silva (2016), have suggested that the performance of parallel kinematic manipulators may be enhanced by the use of kinematic redundancies since they promote a significant reduction in the singularities and homogenization on the actuation forces. Kinematic redundancy can be implemented by the introduction of extra active joints in a kinematic chain. Because of this, the inverse kinematic problem presents infinite solutions, i.e., there are infinite possible joint parameters for a single end effector's pose (Siciliano, 1990). The full capability of several levels of kinematic redundancies can only be assessed by appropriate motion planning and by the design of efficient model-based control strategies. Both methodologies rely on the use of validated kinematic and dynamic models.

To take better advantage of its potential, parallel manipulators requires a precise and fast calculation of the dynamic equations of motion. This can be only accomplished by an accurate estimation of the inertia and friction parameters (Thanh et al., 2012).

It is common sense that the dynamics of manipulators can be directly derived form their structure and geometry, i.e., their dynamic parameters. Some of these parameters can be obtained from suppliers or by computer-aided design software (CAD). However, this is not straightforward for parallel kinematic machines containing many components and interactions. In these cases, parameter identification techniques should be exploited.

This paper adresses the dynamic modeling and identification of a planar parallel kinematic manipulator (PKM) with

several levels of kinematic redundancies, the 3PRRR. As commonly used in the field of parallel robots, the letter R corresponds to revolute joints, the letter P to prismatic joints, the underlined letter to actuated joints and the number in front of the name refers to the number of kinematic chains. The end-effector of this planar manipulator is considered a rigid body which can move in a plane, yielding a system with three DOFs. The actuation of these DOFs is done by six servomotors: three moving three linear guides (P) and three moving links (R). In this way, this PKM presents three levels of kinematic redundancies.

A 3PRRR prototype, depicted in Fig. 1, was built at São Carlos School of Engineering – University of São Paulo. The actuators are Maxon DC motors connected to digital positioning controllers. The connection between these controllers is via CAN protocol. The human machine interface is implemented in two ways: (i) via Matlab and USB communication and (ii) via Matlab/Simulink and DSpace/CAN communication. Its kinematic and dynamic modeling is described in the following section. After that, the parameter identification approach is described. Results and conclusions are finally addressed.

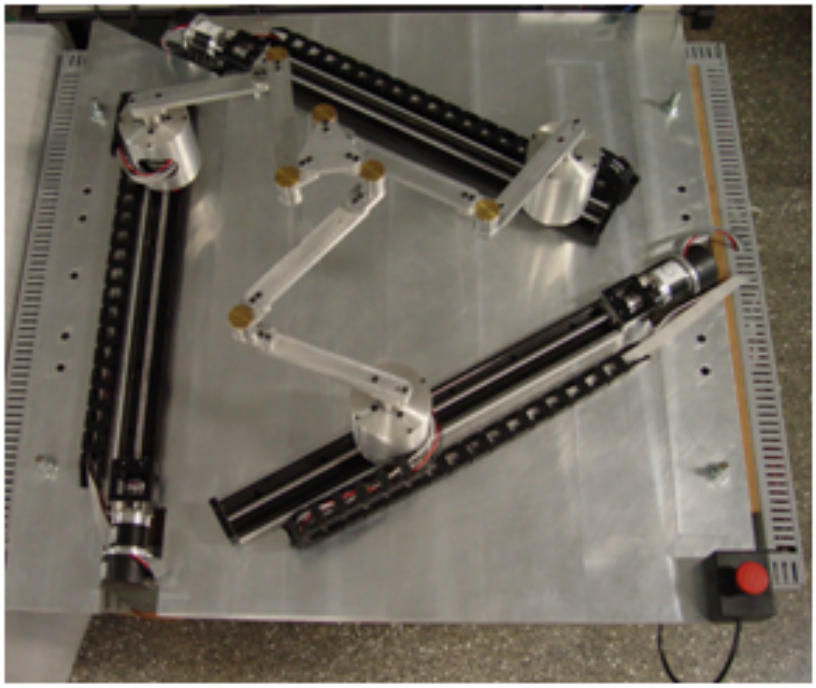

Figure 1 – The 3PRRR prototype.

KINEMATIC MODEL

In this section, it is presented the formulation to obtain the model of the 3PRRR manipulator. Figure 2 illustrates a scheme of the geometry of the 3PRRR. The subscript $i = 1,2,3$ describes the kinematic chain. There are rotary joints in A_i, B_i and C_i, where A_i is active and B_i and C_i are passive. The angles θ_i and β_i represent the orientation of A_iB_i and B_iC_i, respectively. The lengths of links A_iB_i and B_iC_i are, respectively, l_1 and l_2. Linear actuators, in A_i, have their position in ζ_i and orientation of γ_i. The distance between robot's center and the central position of the linear actuators is represented by a. The Cartesian position of the end effector is (x,y) with orientation α. The distance of C_i to the center of the end effector is h.

Inverse Kinematics

The inverse kinematic model is used to determine the actuators' parameters $\boldsymbol{\Theta} = [\theta_1, \theta_2, \theta_3, \zeta_1, \zeta_2, \zeta_3]^T$ that yield a desired end-effector's position $\boldsymbol{X} = [x, y, \alpha]^T$. Due to 3PRRR kinematic redundancies, this task is not simple since the mechanism presents six actuators while the end-effector presents only three DOFs. As a consequence, this problem, usually denoted as redundancy resolution, presents infinity solutions. The selection among these possible solution can be derived by the definition of the linear actuators' positions ζ_1, ζ_2 and ζ_3.

First, the variables ρ_{xi} and ρ_{yi} are denoted as:

$$\begin{bmatrix} \rho_{xi} \\ \rho_{yi} \end{bmatrix} = \begin{bmatrix} x + h\cos(\alpha + \gamma_i \pm \frac{\pi}{2}) - \zeta_i \cos(\gamma_i) - a\cos(\gamma_i \pm \frac{\pi}{2}) \\ y + h\sin(\alpha + \gamma_i \pm \frac{\pi}{2}) - \zeta_i \sin(\gamma_i) - a\sin(\gamma_i \pm \frac{\pi}{2}) \end{bmatrix}. \tag{1}$$

Then, in order to eliminate β_i, the following equation is used

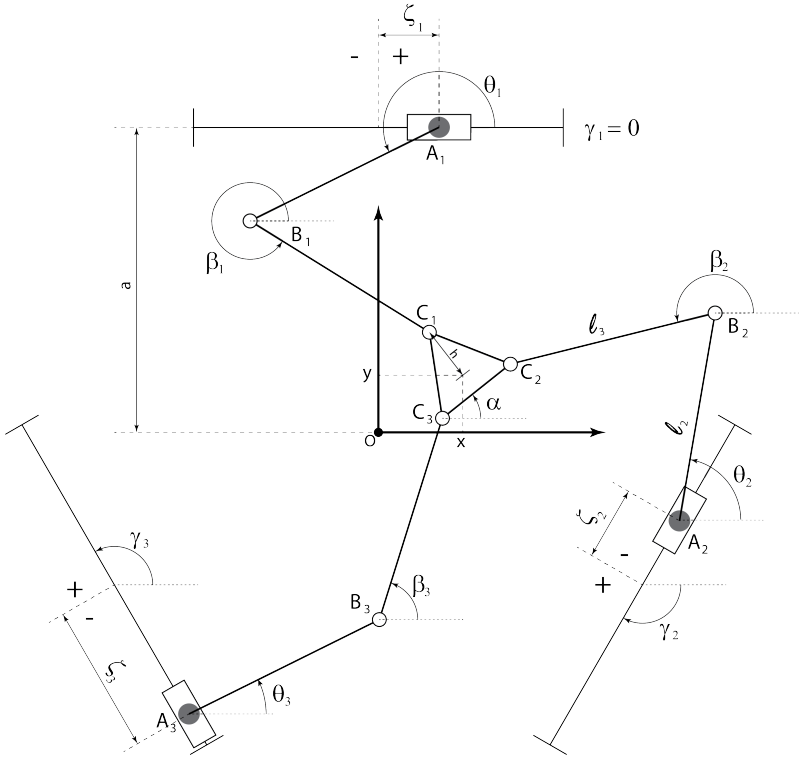

Figure 2 – Geometric scheme of the 3PRRR.

$$\left\|\mathbf{r}_{\mathbf{C_i}} - \mathbf{r}_{\mathbf{B_i}}\right\| = \left\| \begin{array}{c} \mu_i - l_1\cos(\theta_i) \\ \rho_i - l_1\sin(\theta_i) \end{array} \right\|^2 = l_2^2. \tag{2}$$

Expanding the norm in (1) and rearranging its result, the folowing relation is obtained

$$\rho_{xi}^2 + \rho_{yi}^2 + l_1^2 - l_2^2 - 2l_1(\rho_{xi}\cos(\theta_i) + \rho_{yi}\sin(\theta_i)) = 0. \tag{3}$$

For the sake of simplicity, (3) will be represented as

$$k_{i1} + k_{i2}\cos(\theta_i) + k_{i3}\sin(\theta_i) = 0, \tag{4}$$

where

$$\left[\begin{array}{c} k_{i1} \\ k_{i2} \\ k_{i3} \end{array} \right] = \left[\begin{array}{c} \rho_{xi}^2 + \rho_{yi}^2 + l_1^2 - l_2^2 \\ -2l_1\rho_{xi} \\ -2l_1\rho_{yi} \end{array} \right]. \tag{5}$$

Then, the tangent half-angle substitution is employed to solve (4) for θ_i, leading to:

$$\theta_i = 2\arctan\left(\frac{-k_{i3} \pm \sqrt{-k_{i1}^2 + k_{i2}^2 + k_{i3}^2}}{k_{i1} - k_{i2}} \right). \tag{6}$$

Lastly, the angle β_i can be determined by

$$\beta_i = \arctan\left(\frac{\rho_{yi} - l_1\sin(\theta_i)}{\rho_{xi} - l_1\cos(\theta_i)} \right). \tag{7}$$

Jacobian Matrix

The Jacobian Matrix, which relates $\dot{X}$ with $\dot{\Theta}$, needs to be determined as well. One way to determine it is by using the following relation:

$$\|\boldsymbol{r}_{BC}\|^2 = l_2^2. \tag{8}$$

Differentiating (8), results in

$$r_{BC_x}\dot{r_{BC_x}} + r_{BC_y}\dot{r_{BC_y}} = 0. \tag{9}$$

The variables $r_{\dot{BC}_x}$ and $r_{\dot{BC}_y}$ can be determined by the derivative of (3). Since $r_{BC_x} = l_2\cos(\beta_i)$ and $r_{BC_y} = l_2\sin(\beta_i)$, (9) can be rewritten as

$$\dot{x}l_2\cos(\beta_i) + \dot{y}l_2\sin(\beta_i) + \dot{\alpha}l_2 h\sin(\beta_i - \gamma_i - \alpha \pm \frac{\pi}{2}) = \dot{\theta}_1 l_2\sin(\beta_i - \theta_i) + \dot{\zeta}_i l_2\cos(\beta_i - \gamma_i). \tag{10}$$

Denoting $\dot{\mathbf{X}} = [\dot{x}, \dot{y}, \dot{\alpha}]^T$, $\dot{\mathbf{\Theta}} = [\dot{\theta}_1, \dot{\theta}_2, \dot{\theta}_3, \dot{\zeta}_1, \dot{\zeta}_2, \dot{\zeta}_3]^T$ and $\mathbf{A}$ and $\mathbf{B}$ as follows

$$\mathbf{A} = l_2 \begin{bmatrix} \cos(\beta_1) & \sin(\beta_1) & h\sin(\beta_1 - \gamma_1 - \alpha \pm \frac{\pi}{2}) \\ \cos(\beta_2) & \sin(\beta_2) & h\sin(\beta_2 - \gamma_2 - \alpha \pm \frac{\pi}{2}) \\ \cos(\beta_3) & \sin(\beta_3) & h\sin(\beta_3 - \gamma_3 - \alpha \pm \frac{\pi}{2}) \end{bmatrix}, \tag{11}$$

$$\mathbf{B} = l_2 \begin{bmatrix} l_1\sin(\beta_1 - \theta_1) & 0 & 0 & \cos(\beta_1 - \gamma_1) & 0 & 0 \\ 0 & l_1\sin(\beta_2 - \theta_2) & 0 & 0 & \cos(\beta_2 - \gamma_2) & 0 \\ 0 & 0 & l_1\sin(\beta_3 - \theta_3) & 0 & 0 & \cos(\beta_3 - \gamma_3) \end{bmatrix}. \tag{12}$$

Equation (10) can be stated as

$$\mathbf{A}\dot{\mathbf{X}} = \boldsymbol{B}\dot{\mathbf{\Theta}}. \tag{13}$$

The Jacobian Matrix, $\mathbf{J}$ can be defined as

$$\dot{\mathbf{X}} = \boldsymbol{A}^{-1}\boldsymbol{B}\dot{\mathbf{\Theta}}\boldsymbol{J}\dot{\mathbf{\Theta}}. \tag{14}$$

DYNAMIC MODELLING

The dynamic model is developed based on the Euler-Lagrange equations (Fontes and da Silva, 2016). Lagrange Multipliers are employed to deal with the kinematic constraints.

Kinetic Energy

Each kinematic chain i has three rigid bodies. Each body is identified by an index j. The concentrated mass in A_1 is identified by $j = 1$ and the links A_iB_i and B_iC_i by $j = 2$ and $j = 3$, respectively.

The position of each chain is denoted by

$$\mathbf{\Theta}_i^* = \begin{bmatrix} \zeta_i \\ \theta_i \\ \beta_i \end{bmatrix}. \tag{15}$$

The center of mass of the body j of chain i has Cartesian and angular velocities denoted by

$$\boldsymbol{\upsilon}_{ij} = \begin{bmatrix} \upsilon_{xij} \\ \upsilon_{yij} \\ \omega_{ij} \end{bmatrix}. \tag{16}$$

The partial velocity matrix K_{ij} relates υ_{ij} with $\dot{\Theta}_i^*$ as shown in

$$\boldsymbol{\upsilon}_{ij} = \boldsymbol{K}_{ij}\dot{\mathbf{\Theta}}_i^*. \tag{17}$$

Considering s_1 the distance between A_i to the center of mass of the link A_iB_i and s_2 the distance between B_i to the center of mass of the link B_iC_i, the matrices K_{ij} are obtained from (18),(19) and (20).

$$\mathbf{K}_{i_1} = \begin{bmatrix} \cos(\gamma_i) & 0 & 0 \\ \sin(\gamma_i) & 0 & 0 \\ 0 & 0 & 0 \end{bmatrix}, \tag{18}$$

$$\mathbf{K}_{i_2} = \begin{bmatrix} \cos(\gamma_i) & -s_1\sin(\theta_i) & 0 \\ \sin(\gamma_i) & s_1\cos(\theta_i) & 0 \\ 0 & 1 & 0 \end{bmatrix}, \tag{19}$$

$$\mathbf{K}_{i_3} = \begin{bmatrix} \cos(\gamma_i) & -l_1\sin(\theta_i) & -s_2\sin(\beta_i) \\ \sin(\gamma_i) & l_1\cos(\theta_i) & s_2\cos(\beta_i) \\ 0 & 0 & 1 \end{bmatrix}. \tag{20}$$

The parameters of mass and inertia of each body are represented by the matrix

$$\boldsymbol{\mu}_j = \begin{bmatrix} m_j & 0 & 0 \\ 0 & m_j & 0 \\ 0 & 0 & I_j \end{bmatrix}. \tag{21}$$

Since the manipulator is planar, the potential energy V is considered constant. The kinetic energy T_i of each kinematic chain is obtained through the following equation

$$\boldsymbol{T}_i = \frac{1}{2}\sum_{j=1}^{3} \boldsymbol{\upsilon}^T \boldsymbol{\mu}_j \boldsymbol{\upsilon}. \tag{22}$$

Substituting equation (17) into equation (22) results in

$$\boldsymbol{T}_i = \frac{1}{2}\dot{\boldsymbol{\Theta}}_i^{*T} \left(\sum_{j=1}^{3} \boldsymbol{K}_{ij}^T \boldsymbol{\mu}_j \boldsymbol{K}_{ij} \right) \dot{\boldsymbol{\Theta}}_i^*. \tag{23}$$

Denoting the mass and inertia matrix of the end-effector by

$$\boldsymbol{M}_E = \begin{bmatrix} m_{EE} & 0 & 0 \\ 0 & m_{EE} & 0 \\ 0 & 0 & I_{EE} \end{bmatrix}. \tag{24}$$

The end-effector's kinetic energy T_E is obtained by

$$\boldsymbol{T}_E = \frac{1}{2}\dot{\boldsymbol{X}}^T \boldsymbol{M}_E \dot{\boldsymbol{X}}. \tag{25}$$

So, the matrix $\boldsymbol{M}_i$ and the vector $\boldsymbol{q}$ can be defined by

$$\boldsymbol{M}_i = \frac{1}{2}\dot{\boldsymbol{\Theta}}_i^{*T} \left(\sum_{j=1}^{3} \boldsymbol{K}_{ij}^T \boldsymbol{\mu}_j \boldsymbol{K}_{ij} \right) \dot{\boldsymbol{\Theta}}_i^*, \tag{26}$$

$$\boldsymbol{q} = [\boldsymbol{\Theta}_1^{*T} \boldsymbol{\Theta}_2^{*T} \boldsymbol{\Theta}_3^{*T} \boldsymbol{X}^T]^T. \tag{27}$$

In this way, the total kinetic energy can be denoted as

$$\boldsymbol{T} = \frac{1}{2}\dot{\boldsymbol{q}}^T \boldsymbol{M} \dot{\boldsymbol{q}}, \tag{28}$$

where

$$\boldsymbol{M} = \begin{bmatrix} \boldsymbol{M}_1 & \boldsymbol{0} & \boldsymbol{0} & \boldsymbol{0} \\ \boldsymbol{0} & \boldsymbol{M}_2 & \boldsymbol{0} & \boldsymbol{0} \\ \boldsymbol{0} & \boldsymbol{0} & \boldsymbol{M}_3 & \boldsymbol{0} \\ \boldsymbol{0} & \boldsymbol{0} & \boldsymbol{0} & \boldsymbol{M}_E \end{bmatrix}. \tag{29}$$

Dynamic equations

As the system presents 6 active inputs and 12 generalized coordinates $\mathbf{q}$, constraint equations have to be derived. In this way, 6 Lagrange multipliers $\boldsymbol{\lambda} = [\lambda_1 ... \lambda_6]^T$ and 6 constraint equations are needed. The constraints are given by the following geometrical relations:

$$\mathbf{g} = \begin{bmatrix} x + h\cos(\alpha + \gamma_1 \pm \frac{\pi}{2}) - \zeta_1 \cos(\gamma_1) - a\cos(\gamma_1 \pm \frac{\pi}{2}) - l_1 \cos(\theta_1) \\ y + h\sin(\alpha + \gamma_1 \pm \frac{\pi}{2}) - \zeta_1 \sin(\gamma_1) - a\sin(\gamma_1 \pm \frac{\pi}{2}) - l_1 \sin(\theta_1) \\ x + h\cos(\alpha + \gamma_2 \pm \frac{\pi}{2}) - \zeta_2 \cos(\gamma_2) - a\cos(\gamma_2 \pm \frac{\pi}{2}) - l_1 \cos(\theta_2) \\ y + h\sin(\alpha + \gamma_2 \pm \frac{\pi}{2}) - \zeta_2 \sin(\gamma_2) - a\sin(\gamma_2 \pm \frac{\pi}{2}) - l_1 \sin(\theta_2) \\ x + h\cos(\alpha + \gamma_3 \pm \frac{\pi}{2}) - \zeta_3 \cos(\gamma_3) - a\cos(\gamma_3 \pm \frac{\pi}{2}) - l_1 \cos(\theta_3) \\ y + h\sin(\alpha + \gamma_3 \pm \frac{\pi}{2}) - \zeta_3 \sin(\gamma_3) - a\sin(\gamma_3 \pm \frac{\pi}{2}) - l_1 \sin(\theta_3) \end{bmatrix} = \mathbf{0}. \tag{30}$$

Since the potential energy is constant, the Lagrangian is $\boldsymbol{L} = \boldsymbol{T}$. So, considering $\boldsymbol{\tau} = [\tau_1 ... \tau_{12}]$ the non-conservative generalized forces applied on q_n, $\mathbf{G}$ the Jacobian matrix of constraint equations g and using Euler-Lagrange equations, the following equations are obtained

$$\boldsymbol{M}\ddot{\boldsymbol{q}} + \boldsymbol{b}(\boldsymbol{q}, \dot{\boldsymbol{q}}) + \boldsymbol{G}^T \boldsymbol{\lambda} = \boldsymbol{\tau}, \tag{31}$$

where

$$\boldsymbol{b}(\boldsymbol{q}, \dot{\boldsymbol{q}}) = \dot{\boldsymbol{M}}\dot{\boldsymbol{q}} - \begin{bmatrix} \frac{\partial \boldsymbol{L}}{\partial q_1} \\ \frac{\partial \boldsymbol{L}}{\partial q_2} \\ \vdots \\ \frac{\partial \boldsymbol{L}}{\partial q_{12}} \end{bmatrix}. \tag{32}$$

Inverse Dynamics

The inverse dynamic model is exploited to the evaluation of the required actuator's forces/torques $\boldsymbol{\tau}$ to obtain the desired movement (i.e. $\boldsymbol{q}$, $\dot{\boldsymbol{q}}$ and $\ddot{\boldsymbol{q}}$). Since $\boldsymbol{\tau}$ has 6 nonzero elements (i.e. $\tau_1, \tau_2, \tau_3, \tau_4, \tau_5, \tau_6$), $\boldsymbol{\lambda}$ can be determined using lines 3, 6, 9, 10, 11 and 12 of (31). In this way, the following matrix $\boldsymbol{N}_{ij}(6,12)$ can defined as

$$\boldsymbol{N}_{ij} = \begin{cases} 1 & if \quad j \neq 1,2,4,5,7,8 \\ 0 & if \quad j = 1,2,4,5,7,8 \end{cases} \tag{33}$$

Then, pre-multiplying (31) by $\mathbf{N}$ and solving the result for $\boldsymbol{\lambda}$ leads to

$$\boldsymbol{\lambda} = -(\boldsymbol{N}\boldsymbol{G}^T)^{-1}\boldsymbol{N}(\boldsymbol{M}\ddot{\boldsymbol{q}} + \boldsymbol{b}(\boldsymbol{q}, \dot{\boldsymbol{q}})). \tag{34}$$

Lastly, the torques are obtained by substituting (34) in (31), which results in

$$\boldsymbol{\tau} = \boldsymbol{M}\ddot{\boldsymbol{q}} + \boldsymbol{b}(\boldsymbol{q}, \dot{\boldsymbol{q}}) - \boldsymbol{G}^T(\boldsymbol{N}\boldsymbol{G}^T)^{-1}\boldsymbol{N}(\boldsymbol{M}\ddot{\boldsymbol{q}} + \boldsymbol{b}(\boldsymbol{q}, \dot{\boldsymbol{q}})). \tag{35}$$

IDENTIFICATION OF THE DYNAMIC PARAMETERS

The main objective of the study described in this work is the identification of the inertia values of the manipulators' links and linear actuators. In fact the procedure attempt to estimate the masses m_{l1} and m_{l2} of the links, the mass m_n of the end-effector and the masses m_c of the linear actuators. In order to do that, the procedure is divided in three steps: (i) the selection of the excitation trajectories, (ii) the identification of the inertia parameters using an optimization procedure and (iii) the evaluation of the identification procedure.The following subsections describe these steps. During the trajectories execution, the actuators' positions and currents have been acquired using a frequency of 0.25 kHz.

Excitation trajectories

Two kind of excitation trajectories are exploited. The first one is used to the identification of the linear actuators' masses (m_c). The second one is focused on the determination of the inertia values of the links and the end-effector.

Regarding the first group of trajectories, a single excitation trajectory is employed since the robot is symmetric and m_c is considered to be equal for all linear actuators. In this trajectory, the rotary actuators have been fixed in homing positions and the excitation trajectory execute a move along ζ that is composed of three motions: the linear actuator moves from 0.00m to -0.06m, then it goes to $+0.06$m and, finally it goes back to the initial point 0.00m.

All linear actuators are blocked for the second group of excitation trajectories. In this case, the 3PRRR worked as a 3RRR. Five simulations have been performed using five different excitation trajectories (see Fig. 3). All five trajectories have the shape of a square and the same side length and their centers are positioned in the origin O. The first square (i.e. $i = 1$) was aligned with x and y axis. The remaining squares were designed with a rotation of the first square about z axis by an angle $\phi_i (i = 2,3,4,5)$, given by

$$\phi_i = (i-1)10^{\circ}. \tag{36}$$

The acquired data during the experimental campaign was the actuators' positions and the currents. The current data can be transformed in efforts by:

$$\boldsymbol{\tau} = K_m I, \tag{37}$$

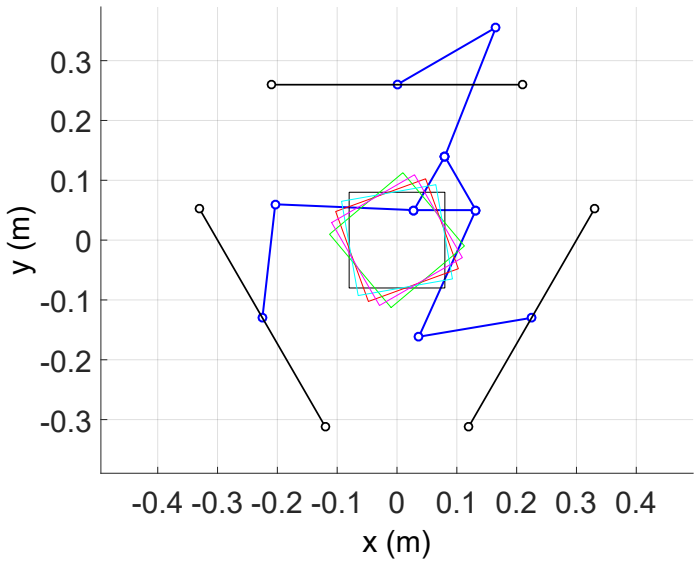

Figure 3 – Excitation squared trajectories.

where K_m is the relation between torque and current of the motors.

Moreover, the required forces to move the linear actuators have to be related to the torque. This relation can be imposed as:

$$\mathbf{F} = \boldsymbol{\tau}\frac{2\pi}{p}, \tag{38}$$

where p is the step of the linear guide for each revolution of the motor.

Considering this, a comparison between the experimental and numerical data can be done. This comparison can be exploited in an optimization scheme for the identification of the inertia values.

Optimization

The identification procedure is performed via an optimization problem. This optimization attempts to minimize the total square error between the experimental $\boldsymbol{\tau}_e$ and the numerical $\boldsymbol{\tau}_t$ inputs. The objective function has been defined as:

$$\begin{aligned} &\boldsymbol{m}_{iopt} = arg\ \ min\left(\sum(\boldsymbol{\tau}_e - \boldsymbol{\tau}_t)^2\right) \\ &subject\ \ to\ \ \boldsymbol{m}_{min} \leq \boldsymbol{m}_{iopt} \leq \boldsymbol{m}_{max}. \end{aligned} \tag{39}$$

The SQP (Sequential Quadratic Programming) algorithm has been employed for solving this problem.

Validation

Finally, the third and last step of the proposed identification procedure is the validation. The validation is performed by the comparison of numerical and experimental data of a different excitation trajectory. This trajectory is defined as an equilateral triangle as shown in Figure 4. Its vertices are $(0, 0.12)$, $(-0.1039, -0.06)$ and $(0.1039, -0.06)$. The pose of the end-effector is defined as $-20°$. This trajectory is performed by moving all actuators (the non-redundant and redundant actuators). The results are described in the next section.

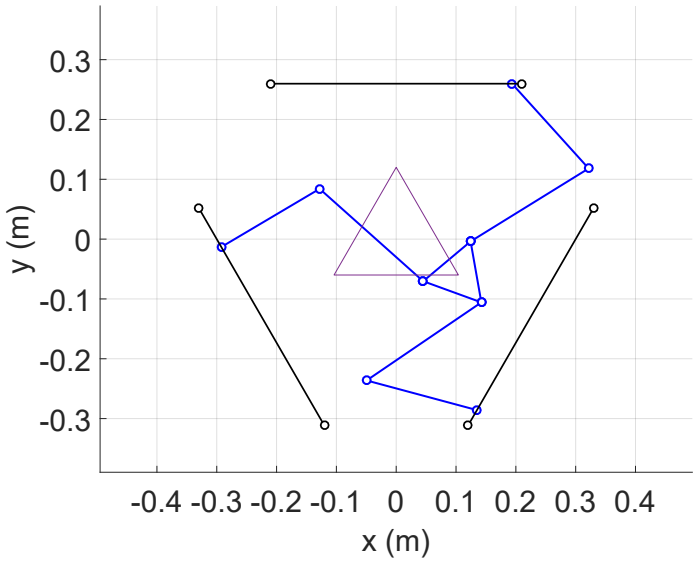

Figure 4 – The triangular validation trajectory.

RESULTS

The optimization solver requires initial values. These values have been defined as the ones found during the design of the manipulator (CAD and manuals). Using these initial values, the optimization procedure was executed and the optimal parameters have been obtained. These values are described in Table 1.

On the one hand, one can notice that three of the four initial values were probably overestimated. On the other hand, the optimization algorithm returned $m_{l1} = 0$ for the A_iB_i link, which can not be true. This can be a suggestion that the model can be done with only one concentrated mass that would represent both links A_iB_i and B_iC_i. It is an important information to reduce the complexity of the design of model-based control strategies for this system.

Table 1 – The inertia parameters: initial and optimal values

Mass	Initial Value (kg)	Final Value(kg)
m_c	780	603.62
m_{l1}	0.30	0
m_{l2}	0.354	0.5723
m_n	0.78	0.2269

Figure 5 shows the comparison of the numerical and experimental linear actuator' forces regarding the identification of the masses of the linear actuators. One can notice that the estimated forces present the same shape of the experimental data. However, there are some time intervals where the accuracy is lower. One possible reason for that relies on the fact that the current model does not consider any friction's model.

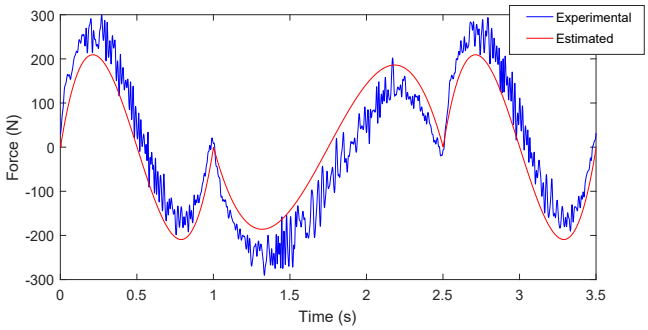

Figure 5 – Comparison between the experimental and the estimated forces considering the identification of the linear actuators' masses

Figure 6 shows the comparison between the experimental and numerical torques of the rotary actuators for the identification of the inertia parameters of the links and the end-effector. The compared inputs are the ones required to perform the fifth square.

In order to validate the identification procedure, a triangular trajectory has been performed using the redundant and non-redundant actuators. The values of experimental and numerical torques/forces to perform this trajectory are shown in Fig. 7.

The similarity of the values demonstrates the capability of the exploited methodology. Nevertheless, improvements

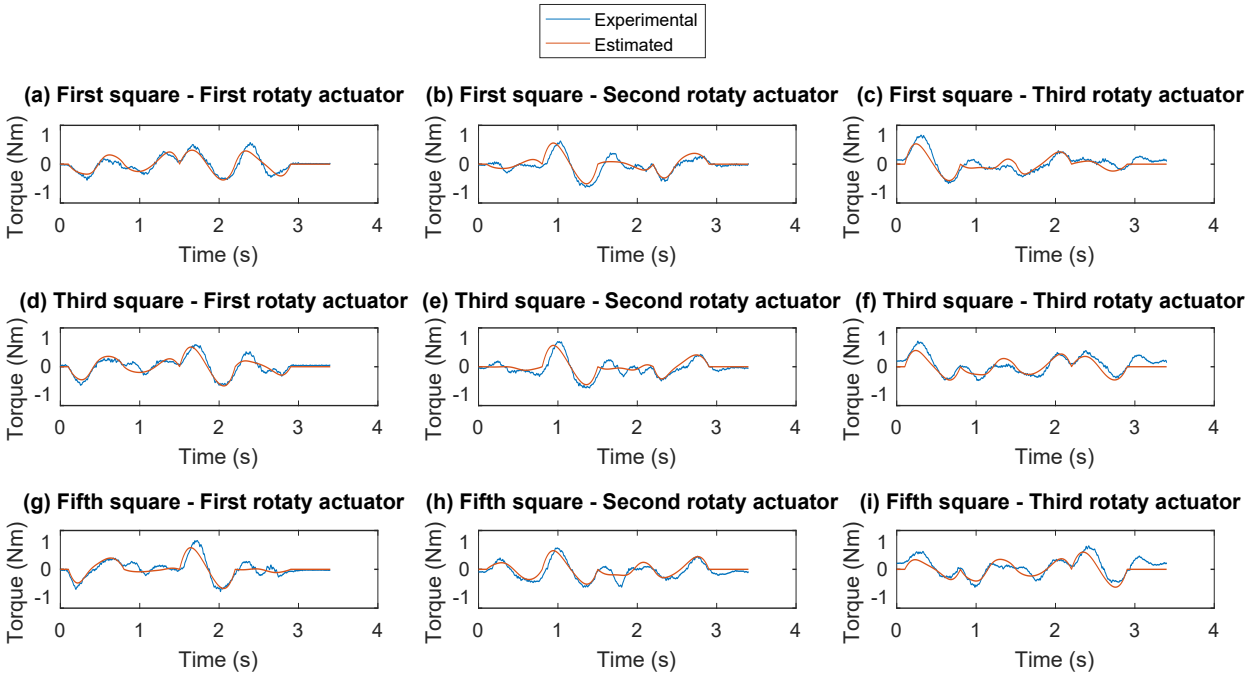

Figure 6 – Comparison between the experimental and the estimated torques considering the identification of the masses of the links and the end-effector

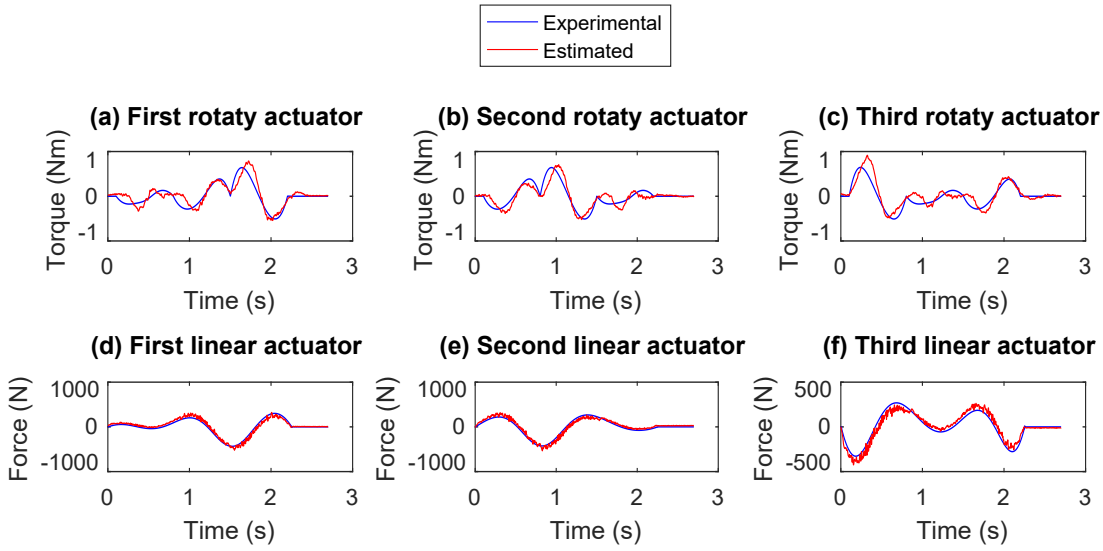

Figure 7 – Comparison between the experimental and the estimated torques/forces required to perform the triangular trajectory

in this optimization procedure can be done by considering noise filtering strategies, different trajectories and control strategies.

CONCLUSIONS

The current work has presented an approach for dynamic modelling and inertia parameter identification of a kinematically redundant planar manipulator 3PRRR.

The dynamic modelling strategy was based on the Euler-Lagrange formalism and the usage of Lagrange multipliers for the constraints' inclusion. The usage of the inertia values derived from CAD models and manuals yielded unsatisfactory correlations between the numerical and experimental data.

A identification procedure for inertia parameters' estimation has been proposed. Different trajectories have been used for the comparison between numerical and experimental data. The difference between this data was used in an optimization for the parameters' estimation. The approach was able to deliver reasonable inertia values. The null inertia value of some links indicates that simpler models can be used during model-based control design strategies.

Future work will include noise filtering strategies, different trajectories (using multisine techniques) and control strategies for the identification procedure.

REFERENCES

Bonev, I. A., Zlatanov, D., and Gosselin, C. M. (2003). Singularity Analysis of 3-DOF Planar Parallel Mechanisms via Screw Theory. *Journal of Mechanical Design*, 125(3):573–581.

Bourbonnais, F., Bigras, P., and Bonev, I. A. (2015). Minimum-time trajectory planning and control of a pick-and-place five-bar parallel robot. *IEEE/ASME Transactions on Mechatronics*, 20(2):740–749.

Cha, S.-H., Lasky, T. A., and Velinsky, S. A. (2007). Singularity Avoidance for the 3-RRR Mechanism Using Kinematic Redundancy. In *Proceedings 2007 IEEE International Conference on Robotics and Automation*, pages 1195–1200, Rome, Italy. IEEE.

Fontes, J. V. and da Silva, M. M. (2016). On the dynamic performance of parallel kinematic manipulators with actuation and kinematic redundancies. *Mechanism and Machine Theory*, 103:148–166.

Gosselin, C. and Angeles, J. (1990). Singularity analysis of closed-loop kinematic chains. *Robotics and Automation, IEEE Transactions on*, 6(3):281–290.

Kotlarski, J., Abdellatif, H., Ortmaier, T., and Heimann, B. (2009). Enlarging the useable workspace of planar parallel robots using mechanisms of variable geometry. In *Reconfigurable Mechanisms and Robots, 2009. ReMAR 2009. ASME/IFToMM International Conference on*, pages 63–72, London, UK.

Lakhal, O., Melingui, A., and Merzouki, R. (2016). Hybrid approach for modeling and solving of kinematics of a compact bionic handling assistant manipulator. *IEEE/ASME Transactions on Mechatronics*, 21(3):1326–1335.

Merlet, J.-P. (1996). Redundant parallel manipulators. *Laboratory Robotics and Automation*, 8(1):17–24.

Mohamed, M. G. and Gosselin, C. M. (2005). Design and analysis of kinematically redundant parallel manipulators with configurable platforms. *Robotics, IEEE Transactions on*, 21(3):277–287.

Paccot, F., Andref, N., and Martinet, P. (2009). Review on the dynamic control of parallel kinematic machines: Theory and experiments. *The International Journal of Robotics Research*, 28(3):395–416.

Ruiz, A. G., Fontes, J. V. C., and da Silva, M. M. (2015). The Impact of Kinematic and Actuation Redundancy on the Energy Efficiency of Planar Parallel Kinematic Machines. In *Proceedings of 17th International Symposium on Dynamic Problems of Mechanics*, Natal , Brazil.

Santos, J. C., Frederice, D., Fontes, J. V. C., and Silva, M. M. D. (2015). Numerical analysis and prototyping details of a planar parallel redundant manipulator. In *2015 12th Latin American Robotics Symposium and 2015 3rd Brazilian Symposium on Robotics (LARS-SBR)*, pages 55–60.

Siciliano, B. (1990). Kinematic control of redundant robot manipulators: A tutorial. *Journal of lntelligent and Robotic Systems*, 3(3):201–212.

Thanh, T. D., Kotlarski, J., Heimann, B., and Ortmaier, T. (2012). Dynamics identification of kinematically redundant parallel robots using the direct search method. *Mechanism and Machine Theory*, 52:277 – 295.

ACKNOWLEDGMENT

This research is supported by FAPESP 2014/01809-0 and FP7-EMVeM (Energy Efficiency Management for Vehicles and Machines). Moreover, Joao C. Santos is grateful for their grant FAPESP 2014/21946-2 and Joao V. C. Fontes and H. L. Vieira are thankful for their CNPq grants.

RESPONSIBILITY NOTICE

The authors are only responsible for the material included in this paper.